Ab Initio Study of the Potential Energy Surfaces for the Reaction C + CH → C_2 + H

M. Boggio-Pasqua, Ph. Halvick,* M.-T. Rayez, and J.-C. Rayez

Laboratoire de Physicochimie Théorique, URA 503-CNRS, Université Bordeaux I, 33405 Talence Cedex, France

J.-M. Robbe

Laboratoire de Dynamique Moléculaire et Photonique, URA 779-CNRS, Université des Sciences et Technologies de Lille, UFR de Physique, 59655 Villeneuve d'Ascq Cedex, France

Received: August 13, 1997; In Final Form: December 1, 1997

The 18 lowest potential energy surfaces of C_2H have been investigated with the complete active space multiconfigurational self-consistent-field method. We restricted our study to the doublet and quartet spin multiplicities. Twelve surfaces are issued from the ground-state reactants, while the six others are issued from the first excited state of the reactants. The approach of C toward CH shows no barrier for 6 of the 12 surfaces, obviously making the reaction possible at very low temperatures. The study of the potential energy curves along the reactant and product channels shows that the X, A, a, b, and c states of C_2 are expected to be populated by the title reaction, even at very low temperatures. Moreover, six new equilibrium structures corresponding to the excited states of C_2H are predicted.

1. Introduction

The study of reaction dynamics, C + CH → C_2H → C_2 + H, beyond its fundamental interest, takes on importance in interstellar chemistry. Indeed, the ethynyl radical C_2H, one of the most abundant polyatomic species in interstellar medium,[1] is a precursor for the formation[2] of C_2, a very reactive chemical species. The C_2H radical also plays an important role in the formation and destruction of carbon compounds, such as carbon chain molecules[3] C_nH which have been detected in interstellar medium for $n = 2-6$. In addition, the C_2H radical is known as the product of some reactions, such as $C_2 + CH_4$[4] or H + C_2H_2,[5] and as the major product of the photodissociation of acetylene.[6]

C_2H was detected in 1964 in argon matrixes[7] and later in the gas phase[8] in 1981. It has been the subject of extensive spectroscopic studies,[7−39] but most of them have focused on the infrared and near-infrared spectra, involving the two lowest-lying states $X^2\Sigma^+$ and $A^2\Pi$. A strong vibronic coupling, due to a conical intersection between the X and A states, make the spectra very complicated. Consequently, the assignments of the vibrationally excited states of C_2H are subject to a large uncertainty.[40,41] The experimental data about the other excited states are rather scarce. There are several studies of vertical absorption spectra, some of which attempt to identify the upper states. Graham et al.[9] observed a band system in the 3000-Å region of the optical spectrum in an argon matrix at 4 K and assigned it to the B($^2\Sigma$ or $^2A'$) ← $X^2\Sigma$ transition. Later, Chang and Graham[11] studied a band system at 1946 Å. However, theoretical works[42−44] were unable to identify the corresponding upper electronic states. Hsu et al.[39,40] studied the UV spectrum of the C_2H radical, using laser-induced fluorescence spectroscopy. They found the upper state at 39 176 cm^{-1} and suggested in their earlier work[39] that it could be the $2^2\Pi$ state. But this was not consistent with the calculations of Duflot et al.,[44] who found the $2^2\Pi$ state at a much higher energy. In a more recent work,[40] Hsu *et al.* supposed that the upper state was not linear and could be the $3^2A'$ state calculated by Shih et al.[42] Let us finally mention a Rydberg state near 9 eV which has been observed by resonance ionization spectroscopy.[37] Theoretical results[44] for this last state are in good agreement with the experimental findings.

Numerous theoretical calculations have been carried out on the ethynyl radical,[43−60] mainly devoted to the understanding of the experimental spectra and generally limited to the $X^2\Sigma^+$ ↔ $A^2\Pi$ transition. Peric, Peyerimhoff, and co-workers have studied the vibronic coupling between the X and *A* states, including spin−orbit effects and hyperfine coupling constants.[53−60] Some information about the other excited states is known through the calculated vertical excitation spectrum.[42−44,48] The potential energy curves published until now are those of Shih and co-workers,[42,48] who tried to assign the absorption spectra and determined the approximate equilibrium geometries for several excited states, and, more recently, those of Duflot and co-workers,[44] who studied extensively the $^2\Sigma^+$ and $^2\Pi$ PES for the C_2H → C_2 + H photodissociation. By using the results of this last work and also the laser-induced fluorescence data, Jackson et al.[61] presented a review of the photodissociation process of the C_2H radical formed under cometary conditions.

Because of the very low interstellar temperatures (10−100 K), only the reactions without barrier or with a very small one can happen in interstellar clouds. We intend in this study to investigate the potential energy surfaces (PES) issued from the reactants C + CH in their ground state in order to have an outline of their topology, especially the possible existence of potential energy barriers during the approach of the reactants. With this aim in view, we calculated some parts of the 12 PES coming from the ground-state reactants. Some other computations for six PES coming from the first excited states of the reactants were also performed, because these PES cross some

* To whom correspondence should be addressed. E-mail: halvick@lpct.u-bordeaux.fr. Fax: +33 556 84 66 45.

S1089-5639(97)02659-5 CCC: $15.00 © 1998 American Chemical Society
Published on Web 02/24/1998

TABLE 1: Dissociation and Excitation Energies (eV) Calculated with the CASSCF, CASPT2, and MRCI Methods[a]

	CASSCF	CASPT2	MRCI	MRCI[g]	expt
D_e(CC−H)	4.588	4.883	5.004	4.948	5.1[b]
D_e(HC−C)	7.745	7.697	7.602	7.467	7.875[c]
ΔE	−3.157	−2.814	−2.598	−2.519	−2.775[d]/−2.684[e]
E(CH $a^4\Sigma^-$) − E(CH $X^2\Pi$)	0.182	0.516	0.681	0.668	0.724[f]
E(C_2 $a^3\Pi_u$) − E(C_2 $X^1\Sigma^+_g$)	0.49	0.117	0.091	0.035	0.087[f]

[a] The ZPE have been discarded from the experimental data. [b] Reference 64. [c] Reference 63. [d] D_e(CC−H) − D_e(HC−C). [e] D_e(C−H) − D_e(C−C). [f] Reference 62. [g] Restricted reference space (see text).

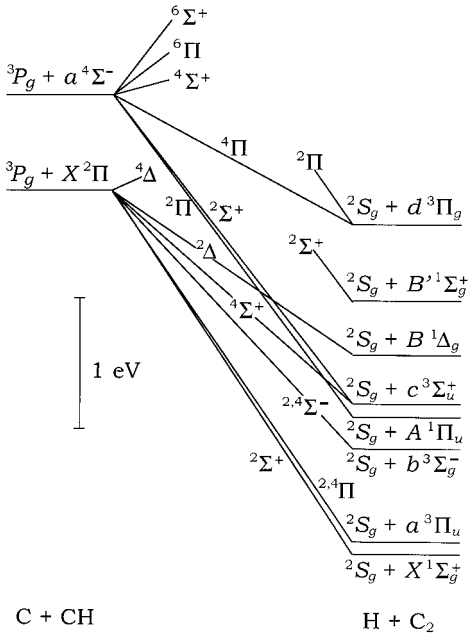

Figure 1. Correlation diagram in $C_{\infty v}$ symmetry.

of the lowest surfaces, thus being coupled via conical intersections. This lead us to compute five $^2A'$ surfaces, four $^2A''$ ones, five $^4A'$ ones, and four $^4A''$ surfaces.

The layout of this paper is as follows. In section 2, we present the correlation diagram. In section 3, we discuss the computational details of the calculations. In section 4, the potential energy surfaces are shown along with the equilibrium structures of the excited states of C_2H. In section 5 are our conclusions.

2. Correlation Diagram

The correlation diagram presented in Figure 1 collects the spectroscopic data available for the atoms and the diatomic species CH and C_2.[62−64] The energy differences correspond to values without the zero-point energies. The potential energy difference between the reactants $C(^3P_g)$ + $CH(X^2\Pi)$ and the products $C_2(X^1\Sigma^+_g)$ + $H(^2S_g)$, both in their ground states, is 2.78 eV, the reaction being exothermic. The excited states $a^3\Pi_u$, $b^3\Sigma^-_g$, $c^3\Sigma^+_u$, and $B^1\Delta_g$ of C_2 are energetically below the ground state of the reactants and are directly correlated to it, when considering $C_{\infty v}$ correlations. There are also two other states of C_2 which are energetically below the ground state of the reactants, namely, the $A^1\Pi_u$ and $B'^1\Sigma^+_g$ states. The $A^1\Pi_u$ state is correlated to the ground states of the reactants only if we consider a C_s correlation. This reveals a conical intersection between the $1^2\Delta$ and $2^2\Pi$ states of C_2H. The $B'^1\Sigma^+_g$ state, which has no direct correlation with the ground and even first excited states of the reactants, is correlated to higher states of the reactants.

3. Computational Details

A reliable description of the PES requires a computational method that accounts for the important electronic rearrangements which occur from the reactants to the products or from ground to excited states. So we have chosen the complete active space self-consistent-field (CASSCF) method. The configurations included in the wave function are obtained by distributing the valence electrons in all possible ways among the valence orbitals, with the constraint to build an eigenfunction of the spin operators S^2 and S_z and the symmetry operators of the C_s point group. The 1s orbitals of the two carbon atoms are kept doubly occupied as they will not participate in the bond breaking and bond forming which occur along the reaction. So for the C_2H molecule, the active space is built with nine electrons distributed in nine orbitals. Each calculation has been achieved by averaging the molecular orbitals on several electronic states of the same symmetry. Then, the wave functions of the different states of the same symmetry differ only by the CI coefficients and not by the MO. It yields a fair description of the ground and excited states and avoids computational difficulties in the regions of PES crossing.

We have also carried out CASPT2 and MRCI calculations in order to know which method is the most suitable for our study. We recall that both methods allow us to account for the dynamic correlation. The CASPT2 method gives a second-order estimation of the difference between the CASSCF energy and the full CI energy. In the MRCI method, the wave function is written as a linear combination of the CASSCF wave function and the configuration state functions which are singly and doubly excited with respect to those of the CASSCF wave function. Then, the CI coefficients are optimized variationally.

The basis set used is the triple-ζ cc-pVTZ basis from Dunning[65] containing p and d polarization orbitals for the hydrogen atom and d and f polarization orbitals for the carbon atom. The calculations have been performed using the program package MOLPRO.[66]

These methods have been used first to calculate the dissociation energies of C−H and C−C bondings in the C_2H radical and the energy difference between the ground states and the first excited states of the reactants and products. The geometry of these species was optimized at the CASSCF level. The results are collected in Table 1 together with experimental data.

It turns out that the CASSCF + MRCI theoretical level yields the best agreement with the experimental results. Nevertheless, this method is very time-consuming, and it would not be convenient to use it for the construction of the full potential surfaces of this system. Therefore, we also tested the MRCI method with a restricted number of configurations in the reference space. Table 2 displays the calculated exoenergicities obtained for different sizes of the reference space. The results show that the reference space can be drastically reduced with little change in the calculated exoenergicity. In Table 1, the fourth column shows the MRCI results obtained with a reference space restricted to the configurations having a weight greater than 0.05 in the CASSCF wave function. The best overall agreement with the experimental values is obtained with the MRCI method using the full CASSCF reference space. The

TABLE 2: Calculated Exoergicity with the MRCI Method, for Different Sizes of the Reference Space (Energies in eV)

threshold	number of CSFs[a]	CPU time,[b] min	exoergicity
0.000	4508	46	2.60
0.005	342	20	2.59
0.01	265	18	2.585
0.03	159	>13	2.56
0.05	124	<13	2.52

[a] Number of configuration state functions in the reference space for C far from CH. [b] CPU time on CRAY J90.

results of lower quality are obtained with the CASPT2 method or with the MRCI method using the restricted reference space.

Therefore, the following calculations of PES have been performed at the CASSCF/cc-pVTZ level which is sufficient for a good qualitative description, while the energies of some important points of the PES have been computed with the MRCI method with the full CASSCF reference space.

4. Results and Discussion

The aim of this work is mainly to identify the PES, issued from the ground states of the reactants, which could display no energy barrier higher than the energy of the reactants along the reaction pathway. Such PES will allow the formation of the products, even at very low temperatures.

4.1. Long-Range Part of the Potential Energy Surfaces. We discuss first the features of the potential energy curves when the carbon atom approaches the diatom CH, just before the formation of the covalent bonding. This is the first region where some energy barriers are expected to occur. The R_{CH} distance was kept constant, at the value of 1.133 Å, the calculated equilibrium geometry of CH($X^2\Pi$). Several values of the bending angle C−C−H (denoted θ) have been investigated. By starting at $\theta = 180°$ (linear CCH) and going to smaller values, we have observed that most of the calculated potential energy curves vs R_{CC} are becoming more and more attractive. For values around 80° for the doublet states and 120° for quadruplet states, all the curves are around their lowest position. Figure 2 shows the energy curves for these two values of θ. We observe that four doublet and two quadruplet PES show no barrier. Thus, along these electronic states, the C_2H molecule can be formed, even at very low temperatures.

4.2. Potential Energy Surfaces of the Doublet States. Let us now investigate the PES in the whole range of nuclear configurations going from the reactants up to the products, to know their topology and, specifically, to know if energy barriers, higher than the energies of the reactants, could occur along the reaction path. The potential energy curves have been computed for several values of the bending angle. We present the results for $\theta = 180°$ and 120°. For each angle, we have computed the C_2H dissociation profile toward C + CH and also toward C_2 + H. In the first case, the C−H distance has been kept to 1.133 Å. In the second one, the C−C distance has been fixed at 1.25 Å. The results of these calculations are collected in Figure 3 for the C + CH approach and Figure 4 for the C_2 + H approach.

We consider first the collinear case, shown in Figure 3a. Four doublet PES come from the reactants in their ground states, namely, the $^2\Pi$, $^2\Sigma^+$, $^2\Sigma^-$, and $^2\Delta$ surfaces. Only the Π one is attractive, the others being repulsive. This behavior can be interpreted if we consider the electronic structure of the reactants, which is represented in Figure 5. The component of the ^{3}P state of carbon with two π electrons leads to the Π states of C_2H. In that case, two electrons are available for the C−C σ bond and three electrons are available for the C−C π bond.

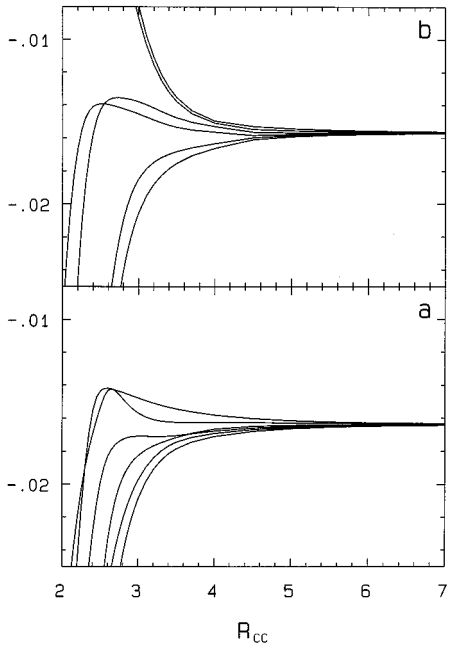

Figure 2. Energies of the doublet (a) and quadruplet (b) states issued from the reactants in their ground state vs the R_{CC} distance. Doublet states are shown for $\theta = 80°$ and $R_{CH} = 1.133$ Å, while quadruplet states are shown for $\theta = 120°$ and $R_{CH} = 1.133$ Å. In this figure and the following ones, energies are given in hartrees and distances in angstroms and the origin of the energies is set at −76.0 hartrees.

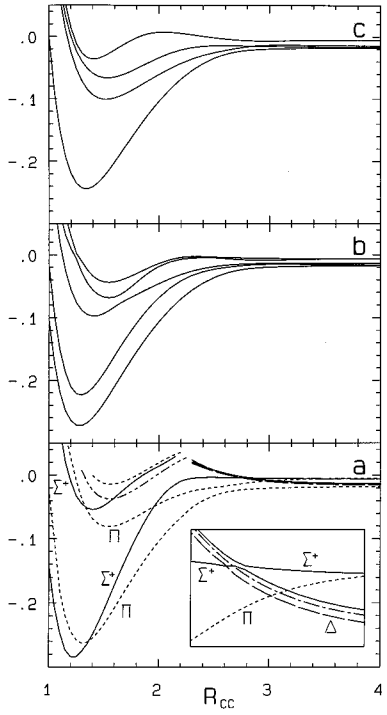

Figure 3. Energies of doublet states vs the R_{CC} distance, shown for $R_{CH} = 1.133$ Å and $\theta = 180°$ (a) and for $\theta = 120°$, ^{2}A′ states (b), ^{2}A″ states (c). In a, continuous lines show Σ^+ states, short dashed lines show Π states, long dashed lines show Δ states, long dash−short dash lines show Σ^-, and long dash−two short dash lines show Φ states. The inset displays a magnified view of the crossings among excited states, in the range $R_{CC} = 2.6$−3.4 Å.

This shows why the $^2\Pi$ and $^4\Pi$ states exhibit an attractive long-range part. The two other components of the ^{3}P state of carbon with one π electron and one σ electron lead to the Σ^+, Σ^-, and Δ states of C_2H. In these last two cases, Figure 5 shows that three electrons are available for the σ bond between the two

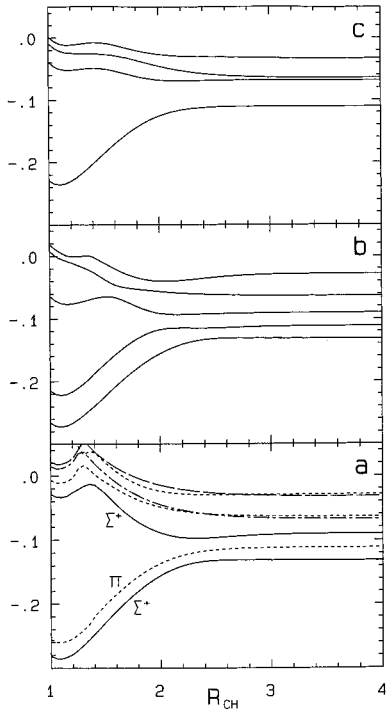

Figure 4. Energies of doublet states vs the R_{CH} distance, shown for $R_{CC} = 1.25$ Å and $\theta = 180°$ (a) and for $\theta = 120°$, $^2A'$ states (b), $^2A''$ states (c). In a, lines have the same meaning as in Figure 3a.

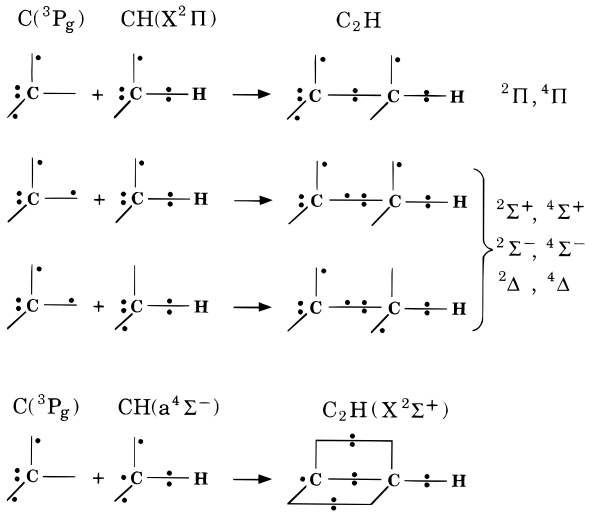

Figure 5. Schematic electronic structures of C_2H built with $C(^3P_g)$ and $CH(X^2\Pi)$ or with $C(^3P_g)$ and $CH(a^4\Sigma^-)$.

carbon atoms. Therefore, an antibonding σ orbital is populated by one electron, thus giving a repulsive nature to the corresponding potential energy surfaces. Figure 3a shows that around $R_{CC} = 3.1$ Å, the repulsive surfaces cross the $^2\Pi$ surface issued from the first excited states of the reactants and around $R_{CC} = 2.8$ Å, they cross the $^2\Sigma^+$ surface issued from the first excited states of the reactants. This lead to an avoided crossing between the $^2\Sigma^+$ curves and to a complicate set of conical intersections, which is, however, significantly higher in energy than the ground states of the reactants. An enlargement of this region is shown in the inset of Figure 3a. Consequently, the $X^2\Sigma^+$ ground state of C_2H, while adiabatically linked to the ground states of the reactants, is *diabatically* linked to the first excited states of the reactants, as long as we consider the collinear configurations of CCH. This can be explained by the electronic structures of the reactants. Figure 5 shows that the electronic structure of the ground state of C_2H cannot come from the ground state of the reactants, while the first excited state of the reactants leads directly to $C_2H(X^2\Sigma^+)$.

At smaller values of R_{CC}, we also see on Figure 3a that the $X^2\Sigma^+$ ground state crosses both $^2\Pi$ states, thus generating two extra conical intersections, which are located at energies below the ground states of the reactants and therefore are expected to influence the dynamics.

Let us now discuss the nonlinear configurations. Figure 3b shows the $^2A'$ states, at $\theta = 120°$, and Figure 3c shows the $^2A''$ states, also at $\theta = 120°$. The main features of the energy curves in that case are not very different from those at $\theta = 180°$. Around equilibrium geometry, there are two A′ curves and one A″ curve which are quite low in energy and well-separated from the higher energy curves. These curves are the A′ and A″ components of the $A^2\Pi$ state and the A′ state corresponding to the $X^2\Sigma^+$ state. Around $R_{CC} = 3$ Å, we observe a narrowing between the energy curves issued from the ground states of reactants and those issued from the first excited states of the reactants. This narrowing indicates the avoided crossings which come from the crossings discussed previously between the energy curves for the collinear configurations. The consequence of these avoided crossings is to generate soft energy barriers on the lowest excited state curves. As was shown previously on Figure 2, these barriers disappear for a smaller bending angle, around 80°. The reason for the favored perpendicular approach of the carbon atom toward CH stems from the fact that the electron of CH available for bonding is in a π orbital. The same effect has been also observed with the reaction N + CH.[67]

The energy curves vs the R_{CH} distance are collected in Figure 4. In the region of small R_{CH} distances, the $X^2\Sigma^+$ and $A^2\Pi$ PES, along with their A′ and A″ components in C_s symmetry, display deep potential wells. They are well-separated from the other PES, which all exhibit a repulsive behavior. If we consider the energy of the ground states of the reactants, around −0.017 hartrees on Figure 3a, we see that the potential energy curves of the excited states in Figure 4 are mainly below that limit, except in the small region at short R_{CH} distances. Moreover, relaxing the R_{CC} distance would lower the energy curves. It is therefore possible to find a reaction pathway on these PES, starting from the ground states of the reactants at low collisional energy and going to the products. Then, all these PES are available for the reaction dynamics. Previously, we have shown that four doublet PES had no barrier opposing to the approach of C toward CH. With the results collected in Figures 3 and 4, we see that no other barrier is present on the reaction pathway on any of these four doublet PES. Among these four states, two are of A′ symmetry and two of A″ symmetry. One A′ state corresponds to the $X^2\Sigma^+$ state of C_2H, one pair (A′, A″) corresponds to the $A^2\Pi$ state, and the last A″ corresponds to the first $^2\Sigma^-$ state. From the correlation diagram, we see that these four doublet PES lead to the $X^1\Sigma^+_g$, $a^3\Pi_u$, and $b^3\Sigma^-_g$ states of C_2. Therefore, these states are expected to be populated by the reaction, even at very low temperatures. Now, if we consider also the electronic transitions which may be induced by the conical intersections, more states will be populated. In Figure 3a, there is a crossing between the $X^2\Sigma^+$ potential energy curve and the second $^2\Pi$ one, around $R_{CC} = 2$ Å. Then, this second $^2\Pi$ curve crosses the second $^2\Sigma^+$ curve around $R_{CC} = 1.3$ Å. Both crossings are below the energy of the ground-state reactants. Thus, we may expect the participation of the $2^2\Sigma^+$ and the $2^2\Pi$ states to the dynamics of the reaction, leading to the production of $C_2(A^1\Pi_u)$ and $C_2(c^3\Sigma^+_u)$.

TABLE 3: Calculated Geometries and Vibrational Frequencies of the First Eight States of C_2H[a]

states	R_{CH}	R_{CC}	θ	ν_1 C−H stretching	ν_2 bending	ν_3 C−C stretching	T_e^{CASSCF}	T_e^{MRCI}
$X^2\Sigma^+$	1.074 (1.041[b])	1.222 (1.216[b])	180.0	3353 (3612[c])	489 (375[d])	1975 (1848[c])	0	0
$A^2\Pi$	1.061 (1.060[e])	1.299 (1.289[e])	180.0	3505(3100[g])	1810/1141(451[e])	1675 (1560[f])	0.92	0.48 (0.46[g]/0.45[h])
$1^4A''$	1.120	1.479	117.7	2801	844	1132	4.10	3.82
$1^4A'$	1.101	1.381	128.0	2982	984	1388	3.80	3.84
$1^4\Pi$	1.090	1.541	180.0	3151	2118/*i*1813	1013	5.05	4.65
$2^2A''$	1.121	1.510	120.2	2774	833	1022	5.36	4.83
$3^2A'$	1.128	1.403	117.9	2666	903	1305	5.36	4.93
$2^4A''$	1.113	1.408	128.2	2795	958	1380	5.36	5.08

[a] Distances are given in Å, frequencies in cm^{-1}, and energies in eV. The experimental values are displayed in parentheses. [b] Reference 31. [c] References 22−24. [d] Reference 15. [e] Reference 37. [f] Reference 9. [g] References 14−16. [h] References 18 and 19. [i] Reference 69.

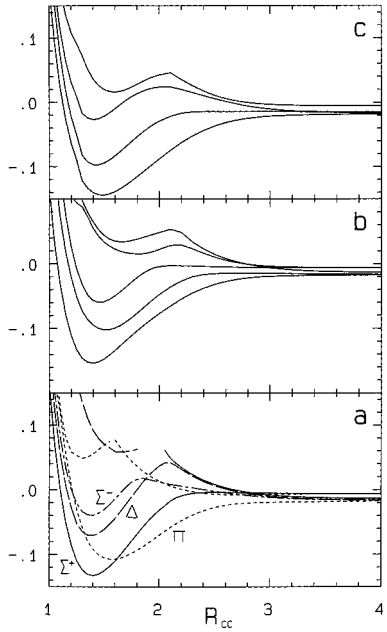

Figure 6. Energies of quadruplet states vs the R_{CC} distance, shown for R_{CH} = 1.133 Å and θ = 180° (a) and for θ = 120°, $^4A'$ states (b), $^4A''$ states (c). In a, lines have the same meaning as in Figure 3a.

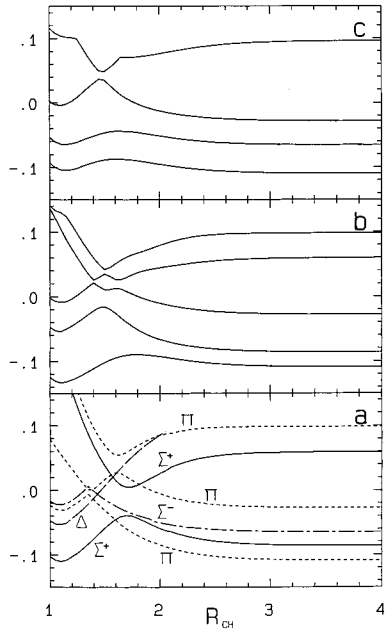

Figure 7. Energies of quadruplet states vs the R_{CH} distance, shown for R_{CC} = 1.25 Å and θ = 180° (a) and for θ = 120°, $^4A'$ states (b), $^4A''$ states (c). In a, lines have the same meaning as in Figure 3a.

4.3. Potential Energy Surfaces of the Quadruplet States. The potential energy curves for the quadruplet states, computed at the same geometries as the doublet states, are shown in Figure 6 for the C + CH approach and in Figure 7 for the C_2 + H approach. Figure 6a shows the potential energy curves vs the R_{CC} distance, for θ = 180°. We observe that several states possess a potential well. However, these wells are not as deep as those of the lowest doublet PES. Again, as mentioned before for the doublet states, many curve crossings are present, yielding many conical intersections. In Figure 7a, which shows the variation of the potential energy vs the R_{CH} distance, for θ = 180°, there is also a complicate set of crossings. All the lowest potential curves coming out of the products C_2 + H are repulsive and cross potential curves issued from highest excited states of the product, around R_{CH} = 1.6 Å. Of course, in the case of states of the same symmetry, avoided crossings are observed.

In the case of collisions at very low velocities, one $^4A'$ state and one $^4A''$ state will be involved, as shown in Figure 2b. They are the components of the first $^4\Pi$ state which lead to $C_2(a^3\Pi_u)$. In Figure 6a, there is a crossing between the $^4\Pi$ potential energy curve and the first $^4\Sigma^+$ potential energy curve, around R_{CC} = 1.6 Å. Thus, the $^4\Sigma^+$ state may be expected to participate to the reaction dynamics. It leads to $C_2(c^3\Sigma^+_u)$. If we consider higher collision energies, one more $^4A'$ state and one more $^4A''$ state could be taken into account. They correspond to the $^4\Sigma^+$ state previously mentioned and to the $^4\Sigma^-$ state, which lead to $C_2(b^3\Sigma^-_g)$.

The main conclusion of this analysis of the doublet and quadruplet PES is that very low velocity collisions may be expected to produce the three lowest states of C_2 (namely, the X, a, and b states), and if we take into account the possible electronic transitions, two more states (A and c states) can also be produced. Moreover, we cannot exclude the possible production of the higher states of C_2, namely, the B, B′, and d states. But in that case, a more thorough investigation of the PES would be necessary, because the PES and the possible crossings that will be involved in the reaction pathway leading to these states of C_2 are lying around the energy of the ground-state reactants.

4.4. Equilibrium Structures. The lowest energy equilibrium structure is an important element in the knowledge of a PES. We have focused our effort on the low-lying states, especially those we expected to find at an energy lower than or around the ground-state product energy. Four doublet states and four quadruplet states have been selected. The equilibrium geometries of these eight states have been optimized at the CASSCF level. The results are collected in Table 3. The MRCI transition energies have been obtained by using the CASSCF-optimized geometries. For the X and A states, the calculated internuclear distances are close to the experimental ones, except for the CH distance of the X state, which is too large by 0.03 Å. For the excited states above the A state, we observe larger CH and CC distances. The distance increase is particularly pronounced for r_{CC}, with a raise ranging from 0.16 up to 0.29

Å. This is consistent with the fact that all excited states above the A state are built on electronic configurations with the π^* orbital occupied. Three states have been found with a linear structure. They are the X and A states, which are well-known from experiments, and also the $1^4\Pi$ state. Upon bending, this $^4\Pi$ state splits into two components: the A′ component, which is stable, and the A″ one, which is unstable. Therefore, this last A″ surface has a bent equilibrium structure called $1^4A''$, which is the lowest-lying quadruplet state. All other calculated structures are bent, with a bending angle around 120°.

Looking at the transition energies, we show that the X and A states are well-separated from the higher-lying states, by more than 3 eV. The states are grouped within sets of small-energy range. First is the set containing the well-known X and A states. Then, we have the $1^4A''$ and $1^4A'$ pair, with an energy range of only 0.02 eV, and also the ($2^2A''$, $3^2A'$, $2^4A''$) set, lying within a 0.25-eV range.

Peyerimhoff et al.[42] have assessed approximate minima of the C_2H states in studying the potential energy curves vs the bending angle for various electronic states. Our results are in qualitative agreement with their findings. The trends in the CC distance and the bending angle are similar. Some discrepancies appear in the relative positions in the energy of several states. They found the $1^4A'$ lower than the $1^4A''$, as we do with the CASSCF results, while the order is inverted in the MRCI results. They also found the $2^4A''$ lower than the $2^2A''$ and $3^2A'$ states, while our MRCI results give the doublet state lower. However, these inversions occur among states close in energy.

The harmonic vibrational frequencies have been computed at the CASSCF level, using finite differences of the energy gradient. The finite difference step has been carefully selected to obtain stable results. We obtain a qualitative agreement with the experimental results for all frequencies of the X state and for the CC stretching of the A state. But we observe a large discrepancy for the bending frequency of the A state. We give two values, corresponding to the two Renner−Teller components.[68] Our lowest value is more than twice as large as the experimental value. The bending frequencies for the other excited states are also very large, especially for the $1^4\Pi$ state, a result which is questionable. The theoretical level at which the frequencies have been computed may be too low to yield reliable bending frequencies. Because this work focuses more on the understanding of the global PES rather than on the spectroscopy of C_2H, we did not try to obtain the bending frequencies with more efficient methods. The stretching frequencies of the excited states seem more reliable. They follow the expected trend, *i.e.*, decreasing when the corresponding internuclear distance is increasing.

The nature of the B state is still not well-defined. Graham et al.[9] observed transitions between 3.6 and 4.8 eV and assigned them to the B($^2\Sigma$ or $^2A'$) upper state. In their first work,[39] Hsu et al. suggested that the upper state they found at 4.86 eV could be the $2^2\Pi$. In a more recent work,[40] they supposed that it could be bent and that the $3^2A'$ state, theoretically estimated[42] at 4.68 eV, was a good candidate. In our work, we located the $3^2A'$ state at 4.93 eV. Considering that an error around 0.1 eV is not unlikely in the MRCI transition energy, our result would agree with the findings of Hsu et al. but would disagree with those of Graham et al. However, in this last work, a set of vibrational frequencies is proposed ($\nu_1 \approx 2700$ cm^{-1}, $\nu_2 \approx 840$ cm^{-1}, $\nu_3 \approx 1300$ cm^{-1}), which is in qualitative agreement with our results for the $3^2A'$ state. The dispersed fluorescence intensity recorded by Hsu et al.[40] shows a significant intensity only when the lower state possesses bending excitation ($\nu_2 \geq 5$). Considering that the $3^2A'$ state is strongly bent, this is consistent with the necessity of a strong bending in the X state to get large Franck−Condon factors. Hsu et al. have determined the rotational parameters of the B state, from which the geometry can be deduced. However, only two parameters are known precisely. On the basis of the estimated geometry of the $3^2A'$ state by Shih et al.,[42] Hsu et al. constrained the R_{CH} distance to 1.07 Å and obtained $R_{CC} = 1.415$ Å and $\theta = 109.1°$, which is in qualitative agreement with the theoretical estimation of Shih et al. But we propose a more reliable and significantly larger value: $R_{CH} = 1.128$ Å (Table 3). By using the experimental rotational parameters and constraining the R_{CH} distance to 1.128 Å, we obtained $R_{CC} = 1.398$ Å and $\theta = 115.3°$. In a second try, we constrained θ to 117.9° and obtained $R_{CC} = 1.389$ Å and $R_{CH} = 1.161$ Å. In the first case, θ is too small in comparison with the ab initio result of Table 3, while in the second case, R_{CH} is too large. In both cases, the distance R_{CC} is slightly smaller than the ab initio value of Table 3. This agrees with the fact that CASSCF computations yield usually equilibrium geometries slightly larger than the experimental values. Then, the agreement between the ab initio geometry given by Table 3 and the geometry deduced from the rotational parameters is good for R_{CC} but only qualitative for R_{CH} and θ. Table 3 shows that the $2^2A''$ state is located 0.1 eV below the $3^2A'$ state and, thus, is also a good candidate for the B state. The ab initio geometries of these two states are very similar, except for the R_{CC} distance which is 1.51 Å and thus is ∼0.1 Å larger than the R_{CC} value deduced above from the spectroscopic parameters. Accordingly, the C−C stretching frequency of the $2^2A''$ state is 1022 cm^{-1} and, thus, is around 300 cm^{-1} smaller than the value proposed by Graham et al. These considerations show that the calculated features of the $3^2A'$ state display a better agreement with the experimental data than do the $2^2A''$ states. However, the experimental data used here are still uncertain and need confirmation. A definitive assignment would require more work, both from experiment and theory.

5. Conclusion

Extensive CASSCF calculations of the PES of the C + CH reaction have been carried out. These calculations reveal that at least two $^2A'$, two $^2A''$, one $^4A'$, and one $^4A''$ surfaces, all correlated to the ground-state reactants, display no barrier within the approach of C(^3P_g) toward CH($X^2\Pi$). Investigations of the PES along the reactant and product channels lead us to conclude that the C(^3P_g) + CH($X^2\Pi$) reaction, at low temperatures, can populate the $X^1\Sigma^+_g$, $A^1\Pi_u$, $a^3\Pi_u$, $c^3\Sigma^+_u$, and $b^3\Sigma^-_g$ states of C_2. A more thorough survey, including the research of the CC−H dissociation saddle points, would be necessary to determine if additional states of C_2 could be produced by this reaction.

All the equilibrium structures of C_2H lying below or around the energies of the ground-state products have been determined. The MRCI transition energies have been calculated and are expected to be accurate. The comparison of our ab initio results for the $3^2A'$ state and the experimental data for the B state yields good agreement. This confirms the previous hypothesis.[40]

In light of these results, it appears that the C + CH reaction evolves in a rather complicated way. Many PES are involved, and they are almost all coupled together either by Renner−Teller effects or by conical intersections. The calculation of the electronic branching ratio among states of C_2 should be a very demanding task, especially if one wants to take into account all the nonadiabatic couplings between the PES.

References and Notes

(1) Ziurys, L. M.; Saykally, R. J.; Plambeck, R.; Erickson, N. *Astrophys. J.* **1974**, *193*, L115.
(2) Van Dishoeck, E. F.; Black, J. H. *Astrophys. J.* **1982**, *258*, 533.
(3) Suzuki, H. *Astrophys. J.* **1983**, *272*, 579.
(4) Richardson, S. L.; Francisco, J. S. *Mol. Phys.* **1994**, *83*, 1041.
(5) Fang, D.-C.; Fu, X.-Y. *Int. J. Quantum Chem.* **1994**, *49*, 3.
(6) Zhang, J.; Riehn, C. W.; Dulligan, M.; Wittig, C. *J. Chem. Phys.* **1995**, *103*, 6815.
(7) Cochran, E. L.; Adrian, F. J.; Bowers, V. A. *J. Chem. Phys.* **1964**, *40*, 213.
(8) Sastry, K. V. L. N.; Helminger, P.; Charo, A.; Herbst, E.; DeLucia, F. C. *Astrophys. J.* **1981**, *251*, L119.
(9) Graham, W. R.; Dismuke, K. I.; Weltner, W., Jr. *J. Chem. Phys.* **1974**, *60*, 3817.
(10) Jinguji, M.; McDowell, C. A.; Shimokoshi, K. *J. Mol. Struct.* **1985**, *130*, 317.
(11) Chang, K. W.; Graham, W. R. M. *J. Chem. Phys.* **1982**, *76*, 5238.
(12) Saykally, R. J.; Veseth, L.; Evenson, K. M. *J. Chem. Phys.* **1984**, *80*, 2247.
(13) Brown, J. M.; Evenson, K. M. *J. Mol. Spectrosc.* **1988**, *131*, 161.
(14) Carrick, P. G.; Pfeiffer, J.; Curl, R. F.; Koester, E.; Tittel, F. K.; Kasper, J. V. V. *J. Chem. Phys.* **1982**, *76*, 3336.
(15) Carrick, P. G.; Merer, A. J.; Curl, R. F. *J. Chem. Phys.* **1983**, *78*, 3652.
(16) Curl, R. F.; Carrick, P. G.; Merer, A. J. *J. Chem. Phys.* **1985**, *82*, 3479.
(17) Curl, R. F.; Carrick, P. G.; Merer, A. J. *J. Chem. Phys.* **1985**, *83*, 4278.
(18) Yan, W. B.; Hall, J. L.; Stephens, J. W.; Richnow, M. L.; Curl R. F. *J. Chem. Phys.* **1987**, *86*, 1657.
(19) Yan, W. B.; Dane, C. D.; Zeitz, D.; Hall, J. L.; Curl, R. F. *J. Mol. Spectrosc.* **1987**, *123*, 486.
(20) Stephens, J. W.; Yan, W. B.; Richnow, M. L.; Solka, H.; Curl, R. F. *J. Mol. Struct.* **1988**, *190*, 41.
(21) Yan, W. B.; Warner, H. E.; Amano, T. *J. Chem. Phys.* **1991**, *94*, 1712.
(22) Milligan, D. E.; Jacox, M. E.; Abouaf-Marguin, L. *J. Chem. Phys.* **1967**, *46*, 4562.
(23) Jacox, M. E. *Chem. Phys.* **1975**, *7*, 424.
(24) Jacox, M. E.; Olson, W. B. *J. Chem. Phys.* **1987**, *86*, 3134.
(25) Shepherd, R. A.; Graham, W. R. M. *J. Chem. Phys.* **1987**, *86*, 2600.
(26) Gottlieb, C. A.; Gottlieb, E. W.; Thaddeus, P. *Astrophys. J.* **1983**, *264*, 740.
(27) Bogey, M.; Demuynck, C.; Destombes, J.-L. *Astron. Astrophys. J.* **1985**, *144*, L15.
(28) Combes, F.; Boulanger, F.; Encrenaz, P. J.; Gerin, M.; Bogey, M.; Demuynck, C.; Destombes, J.-L. *Astron. Astrophys. J.* **1985**, *147*, L25.
(29) Vrtilek, J. M.; Gottlieb, C. A.; Langer, W. D.; Thaddeus, W. D.; Wilson, R. W. *Astrophys. J.* **1985**, *296*, L35.
(30) Woodward, D. R.; Pearson, J. C.; Gottlieb, C. A.; Guélin, M.; Thaddeus, P. *Astron. Astrophys.* **1987**, *186*, L14.
(31) Bogey, M.; Demuynck, C.; Destombes, J.-L. *Mol. Phys.* **1989**, *66*, 955.
(32) Kanamori, H.; Seki, K.; Hirota, E. *J. Chem. Phys.* **1987**, *87*, 73.
(33) Kanamori, H.; Hirota, E. *J. Chem. Phys.* **1988**, *88*, 6699.
(34) Kanamori, H.; Hirota, E. *J. Chem. Phys.* **1989**, *89*, 3962.
(35) Kawaguchi, K.; Amano, T.; Hirota, E. *J. Mol. Spectrosc.* **1988**, *131*, 58.
(36) Endo, Y.; Kanamori, H.; Hirota, E. *Chem. Phys. Lett.* **1989**, *160*, 280.
(37) Cool, T. A.; Goodwin, P. M. *J. Chem. Phys.* **1991**, *94*, 6978.
(38) Hsu, Y.; Wang, P.; Yang, M.; Papousek, D.; Chen, Y.; Chiang, W. *Chem. Phys. Lett.* **1992**, *190*, 507.
(39) Hsu, Y.; Min Lin, J.; Papousek, D.; Tsai, J. *J. Chem. Phys.* **1993**, *98*, 6690.
(40) Hsu, Y.-C.; Shiu, Y.-J.; Lin, C.-M. *J. Chem. Phys.* **1995**, *103*, 5919.
(41) Forney, D.; Jacox, M. E.; Thompson, W. E. *J. Mol. Spectrosc.* **1995**, *170*, 178.
(42) Shih, S.; Peyerimhoff, S. D.; Buenker, R. J. *J. Mol. Spectrosc.* **1979**, *74*, 124.
(43) Koures, A. G.; Harding, L. B. *J. Phys. Chem.* **1991**, *95*, 1035.
(44) Duflot, D.; Robbe, J.-M.; Flament, J.-P. *J. Chem. Phys.* **1994**, *100*, 1236.
(45) Barsuhn, J. *Astrophys. Lett.* **1972**, *12*, 169.
(46) Hillier, I. H.; Kendrick, J.; Guest, M. F. *Mol. Phys.* **1975**, *30*, 1133.
(47) So, S. P.; Richards, W. C. *J. Chem. Soc., Faraday Trans. 2* **1975**, *71*, 660.
(48) Shih, S.; Peyerimhoff, S. D.; Buenker, R. J. *J. Mol. Spectrosc.* **1977**, *64*, 167.
(49) Fogarasi, G.; Boggs, J. E.; Pulay, P. *Mol. Phys.* **1983**, *50*, 139.
(50) Reimers, J. R.; Wilson, K. R.; Heller, E. J.; Langhoff, S. R. *J. Chem. Phys.* **1985**, *82*, 5064.
(51) Kraemer, W. P.; Roos, B. O.; Bunker, P. R.; Jensen, P. *J. Mol. Spectrosc.* **1986**, *120*, 136.
(52) Largo, A.; Barrientos C. *Chem. Phys.* **1989**, *138*, 291.
(53) Thümmel, H.; Peric, M.; Peyerimhoff, S. D.; Buenker, R. J. *Z. Phys. D* **1989**, *13*, 307.
(54) Peric, M.; Buenker, R. J.; Peyerimhoff, S. D. *Mol. Phys.* **1990**, *71*, 673.
(55) Peric, M.; Peyerimhoff, S. D.; Buenker, R. J. *Mol. Phys.* **1990**, *71*, 693.
(56) Peric, M.; Peyerimhoff, S. D.; Buenker, R. J. *J. Mol. Spectrosc.* **1991**, *148*, 180.
(57) Peric, M.; Reuter, W.; Peyerimhoff, S. D. *J. Mol. Spectrosc.* **1991**, *148*, 201.
(58) Peric, M.; Engels, B.; Peyerimhoff, S. D. *J. Mol. Spectrosc.* **1991**, *150*, 56.
(59) Peric, M.; Engels, B.; Peyerimhoff, S. D. *J. Mol. Spectrosc.* **1991**, *150*, 70.
(60) Peric, M.; Peyerimhoff, S. D.; Buenker, R. J. *Z. Phys. D* **1992**, *24*, 177.
(61) Jackson, W. M.; Blunt, V.; Lin, H.; Green, M.; Olivera, G.; Fink, W. H.; Bao, Y.; Urdahl, R. S.; Mohammad, F.; Zahedi, M. *Astron. Spac. Sci.* **1996**, *236*, 29.
(62) Huber, K. P.; Herzberg, G. *Molecular Spectra and Molecular Structure*, *IV. Constants of Diatomic Molecules*; Van Nostrand Reinhold: New York, 1979.
(63) Ervin, K. M.; Gronert, S.; Barlow, S. E.; Gilles, M. K.; Harrison, A. G.; Bierbaum, V. M.; DePuy, C. H.; Lineberger, W. C.; Ellison, G. B. *J. Am. Chem. Soc.* **1990**, *112*, 5750.
(64) Urdahl, R. S.; Bao, Y.; Jackson, W. M. *Chem. Phys. Lett.* **1991**, *178*, 425.
(65) Dunning, T. H. *J. Chem. Phys.* **1989**, *90*, 1007.
(66) Werner, H. J.; Knowles, P. J.; Almlöf, J.; Amos, R. D.; Deegan, M. J. O.; Elbert, S. T.; Hampel, C.; Meyer, W.; Peterson, K.; Pitzer, R.; Stone, A. J.; Taylor, P. R.; Lindh, R.; Mura, M. E.; Thorsteinsson, T. *MOLPRO* version 96.3, University of Birmingham, 1996.
(67) Rayez, M. T.; Halvick, Ph.; Rayez, J. C.; Millié, Ph.; Lévy, B. *Chem. Phys.* **1994**, *188*, 161.
(68) Lee, T. J.; Fox, D. J.; Schaefer, H. F., III. *J. Chem. Phys.* **1984**, *81*, 356.
(69) Lai, L.-H.; Che, D.-C.; Liu, K. *J. Phys. Chem.* **1996**, *100*, 6376.